Supporting Information

A new strategy for anchoring functionalized graphene hydrogel in carbon cloth network to support lignosulfonate/polyaniline hydrogel as integrated electrodes for flexible high areal-capacitance supercapacitor

Dan Wu, Wenbin Zhong*

College of Materials Science and Engineering, Hunan University, Changsha, 410082, P. R. China

*Corresponding author E-mail: wbzhong@hnu.edu.cn (W. Zhong).

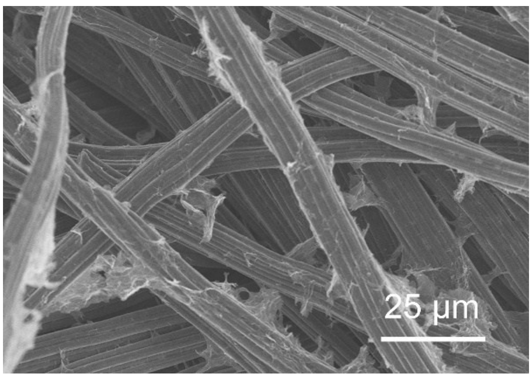

Fig. S1. SEM image of rGO/rOCC.

Preparation of Lig/PANI hydrogel

The lignosulfonate/polyaniline (Lig/PANI) hydrogel was prepared by the in−situ polymerization of aniline (Ani) with the Lig as the crosslinks and dopants. In a typical process, 0.30 g of Lig was first added to 10 mL of deionized water with stirring for 30 min to obtain a transparent solution in an ice bath. 0.45 g (4.8 mmol) Ani was then added into above solution and kept stirring to form homogeneous dispersion, which denoted as solution I. Solution II was prepared by dissolving 1.255 g (5.5 mmol) of ammonium persulfate (APS) in 4 mL deionized water. Subsequently, solution I and II were cooled to 0 °C and mixed quickly with vigorous stirring for 5 s. After standing for 2 h, a stable Lig/PANI hydrogel was formed (Fig. S2).

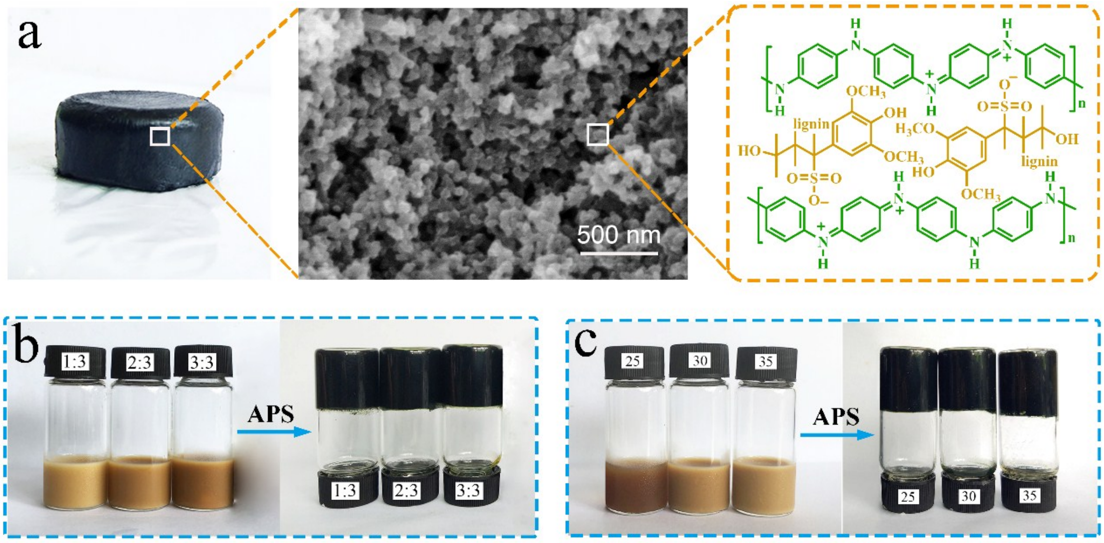

Fig. S2. (a) Lig/PANI at three length-scales. Left: photograph of Lig/PANI hydrogel; middle: a SEM image of Lig/PANI; right: a schematic molecular structure of Lig/PANI. (b) Photographs of the Lig/Ani aqueous dispersion with different mass ratio of Lig to Ani before and after adding APS oxides. (c) Photographs of the Lig/Ani aqueous dispersion with different concentration of Ani (mg mL^{-1}) before and after adding APS.

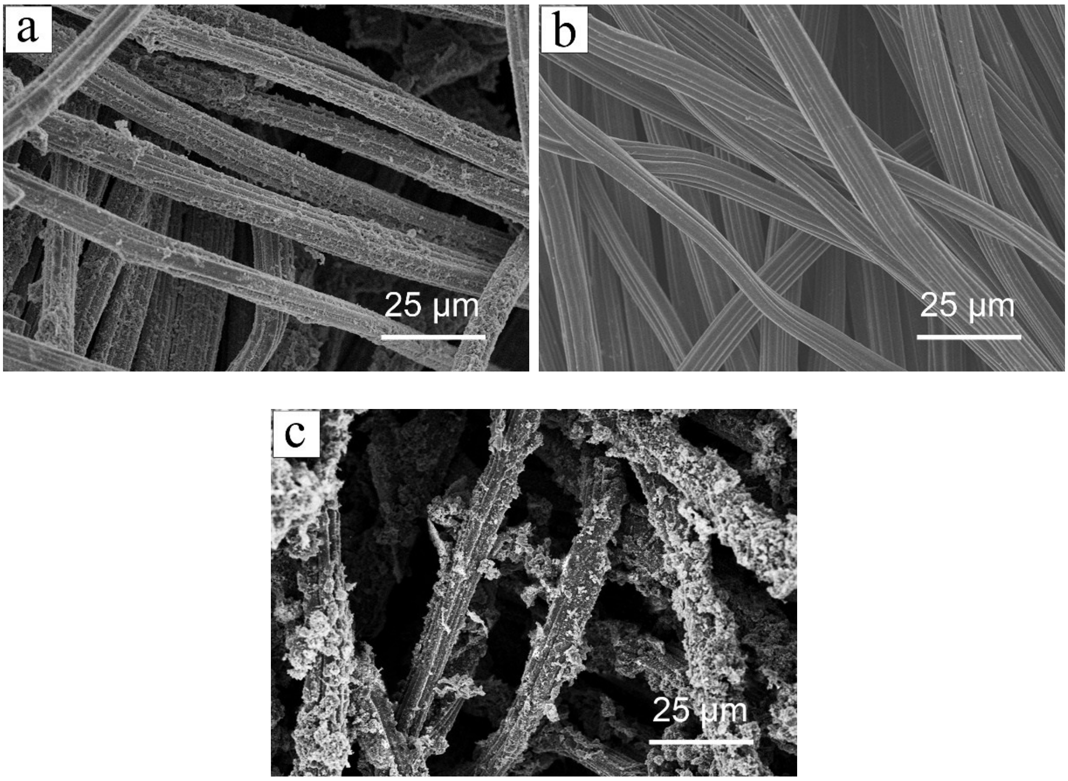

Fig. S3. SEM images of (a) Lig/PANI/rOCC, (b) rOCC and (c) Lig/PANI/rGO/rOCC.

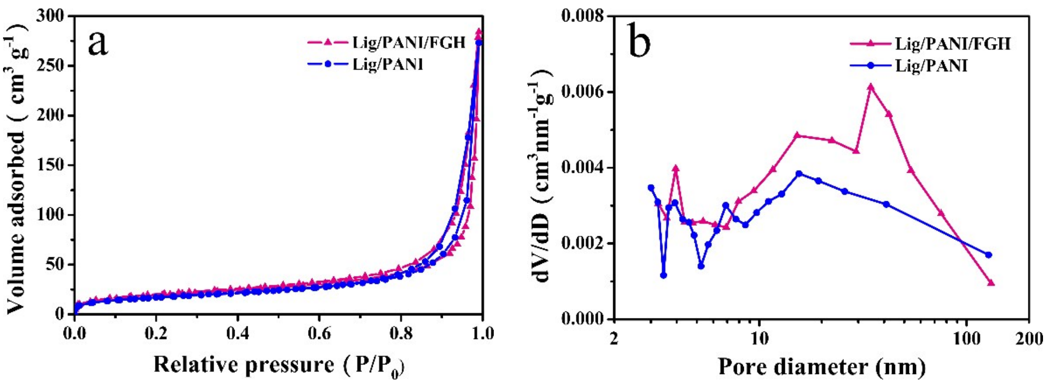

Fig. S4. (a) Adsorption–desorption isotherm curves and (b) the pore size distribution of the Lig/PANI/FGH and Lig/PANI determined by the Barrett-Joyner-Halenda method.

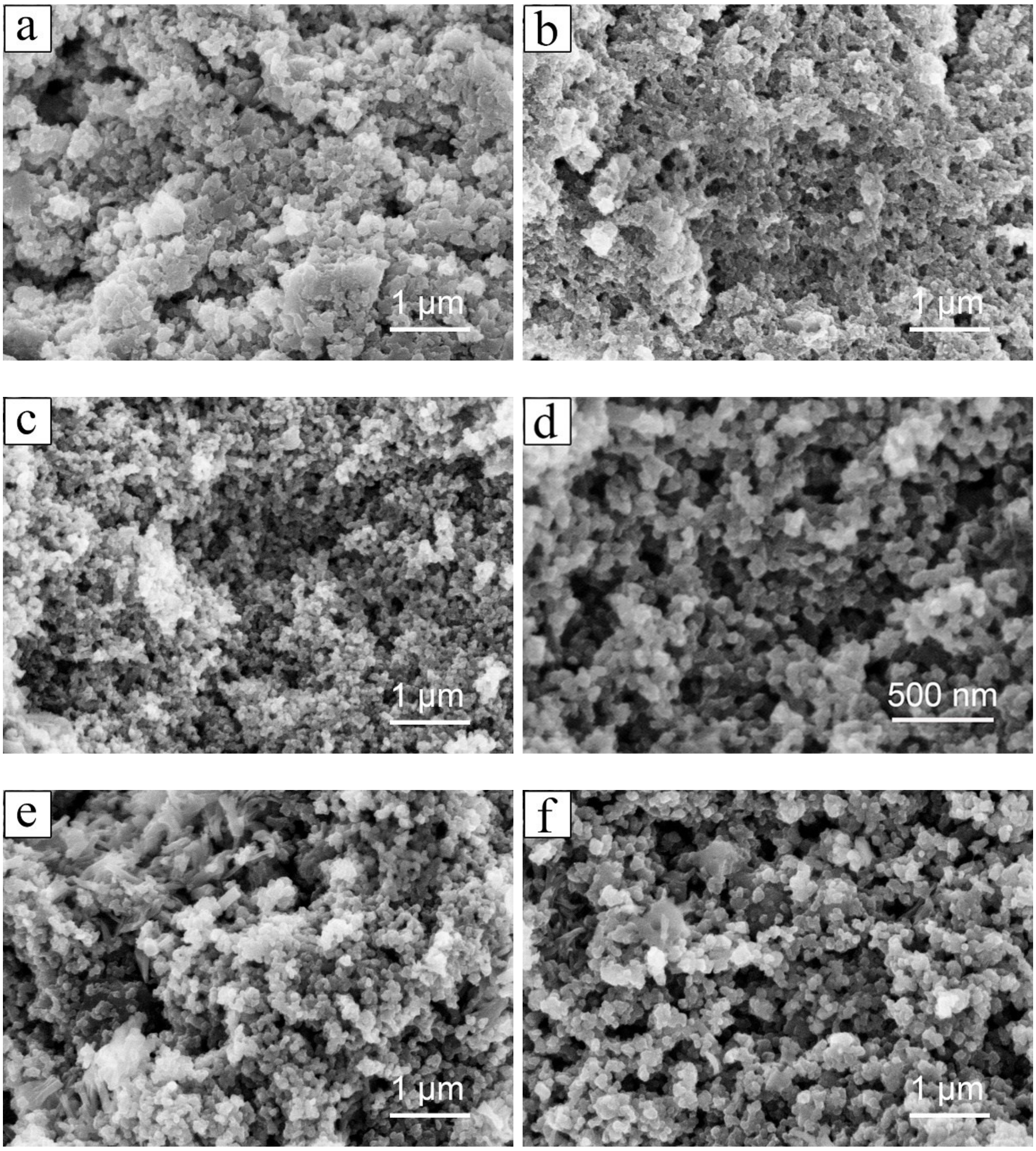

Fig. S5. SEM images of Lig/PANI with different mass ratio of Lig to Ani and concentration of Ani: (a) 1:3, 30 mg mL^{-1}; (b) 3:3, 30 mg mL^{-1}; (c,d) 2:3, 30 mg mL^{-1}; (e) 2:3, 25 mg mL^{-1}; and (f) 2:3, 35 mg mL^{-1}. It is found that the optimized mass ratio of Lig to Ani was 2:3, and the concentration of Ani was 30 mg mL^{-1} to satisfy morphology homogeneity in Lig/PANI hydrogel. Further increasing the Lig:Ani ratio or the concentration of Ani would lead to different degree of aggregation of Lig/PANI nanoparticles.

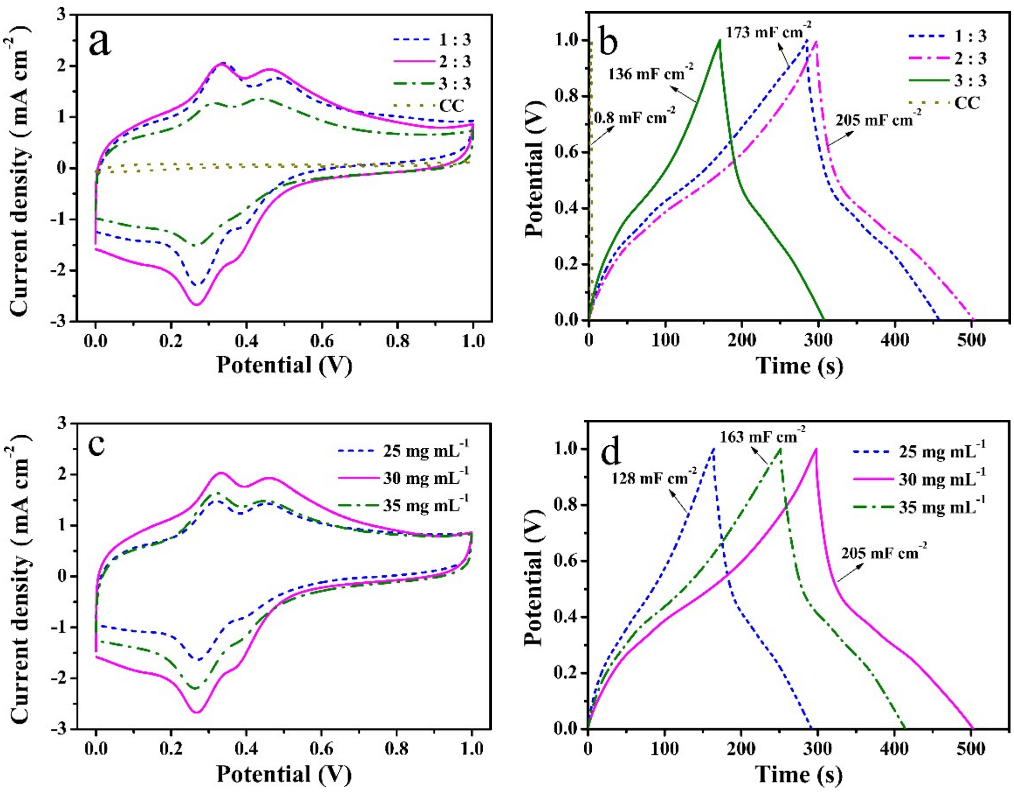

Fig. S6. The electrochemical performance of conventional supercapacitors (1 M H_2SO_4 as electrolyte) based on the Lig/PANI hydrogels prepared with different conditions: (a) CV curves a scan rate of 5 mV s^{-1}, (b) GCD curves at a current density of 1 mA cm^{-2} of Lig/PANI with different mass ratio of Lig to Ani; (c) CV curves a scan rate of 5 mV s^{-1}, (d) GCD curves at a current density of 1 mA cm^{-2} of Lig/PANI with different concentration of Ani.

The corresponding electrodes were prepared identically as that of Lig/PANI/FGH/FCC with FGH/FCC replaced by hydrophilic CC. The hydrophilic CC was treated with 6M HNO_3 at room temperature for 3 days, followed by washing with water and ethanol. It is found that the hydrophilic CC delivers a negligible capacitance and servers as current collector. When the concentration of Ani was 30 mg mL^{-1} and mass ratio of Lig to Ani was 2:3, the corresponding supercapacitor delivers an areal capacitance of 205 mF cm^{-2}, higher than that of others. This result further confirms the optimized mass ratio of Lig to Ani and the concentration of Ani.

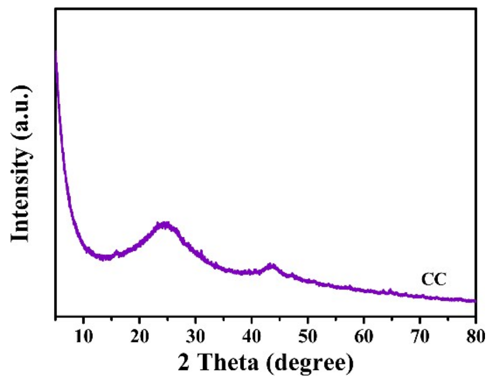

Fig. S7. XRD of the pristine CC.

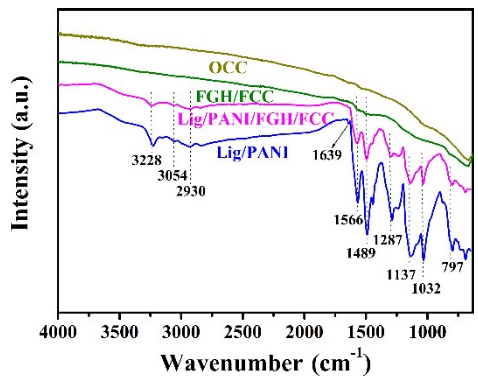

Fig. S8. ATR-FTIR of the OCC, FGH/FCC, Lig/PANI and Lig/PANI/FGH/FCC.

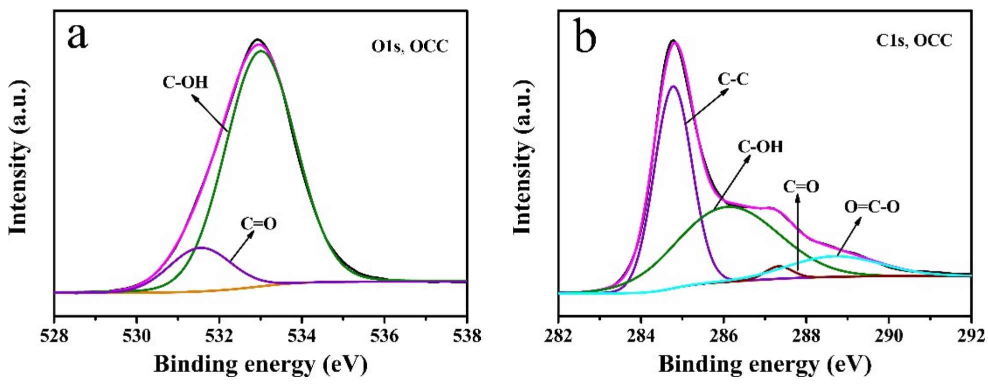

Fig. S9. (a) O1s and (b) C1s core-level spectra of OCC.

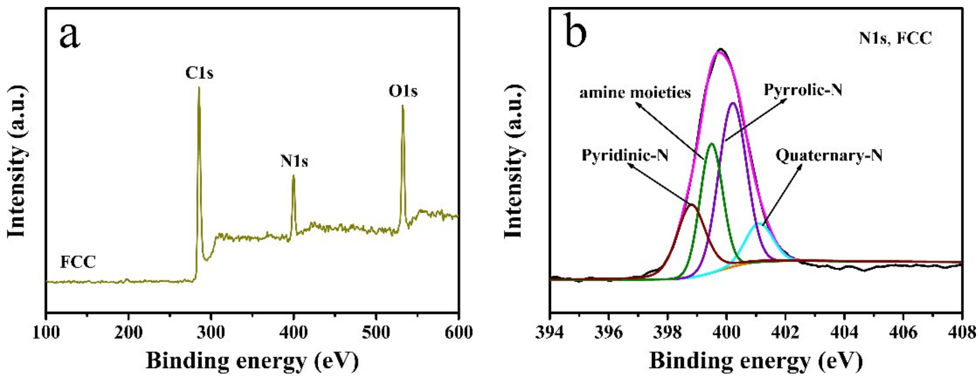

Fig. S10. (a) XPS survey and (d) N1s core-level spectra of FCC.

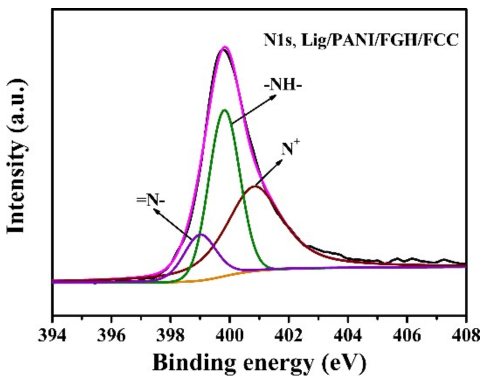

Fig. S11. N1s core-level spectrum of Lig/PANI/FGH/FCC.

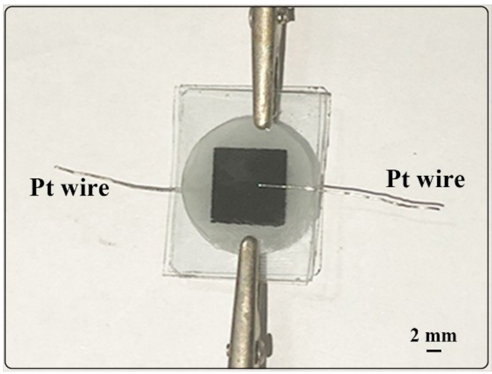

Fig. S12. Photograph of the conventional supercapacitor configuration using 1M H_2SO_4 as electrolyte.

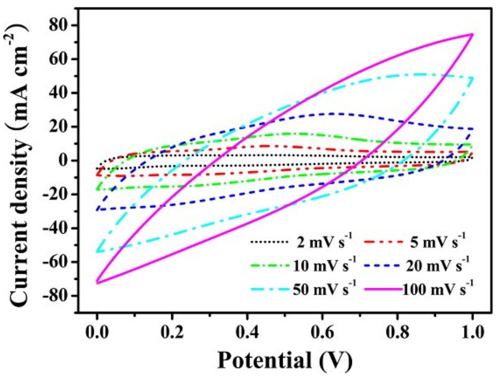

Fig. S13. CV curves of Lig/PANI/FGH/FCC based supercapacitor measured at different scan rates (2~100 mV s^{-1}).

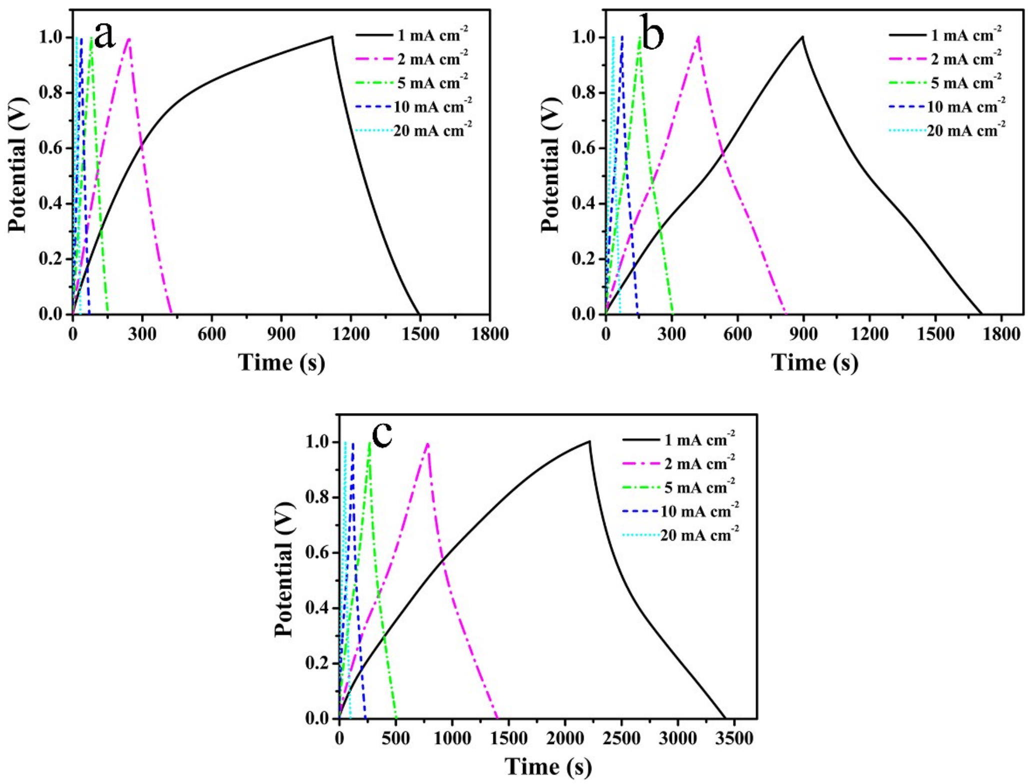

Fig. S14. GCD curves of (a) OCC-based device, (b) FGH/FCC-based device, and (c) Lig/PANI/FGH/FCC-based device at different current densities (1~20 mA cm^{-2}).

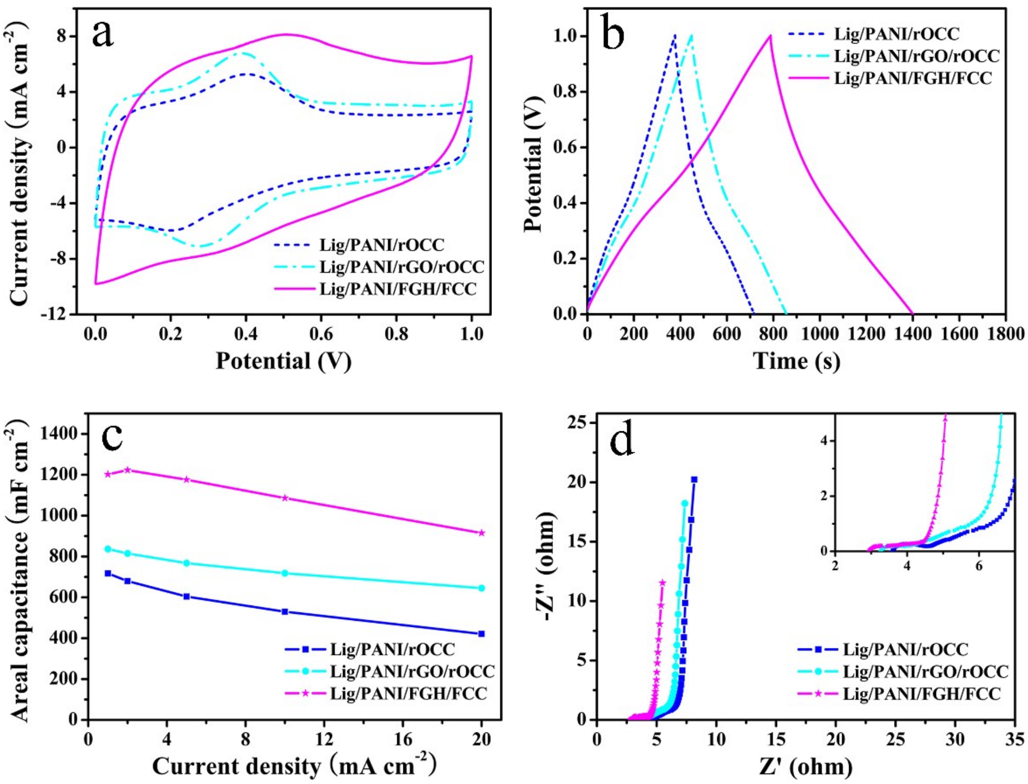

Fig. S15. The comparison of electrochemical performance of the Lig/PANI/rOCC, Lig/PANI/rGO/rOCC, and Lig/PANI/FGH/FCC based supercapacitors using 1M H_2SO_4 as electrolyte: (a) CV curves at a scan rate of 5 mV s^{-1}; (b) GCD curves at a current density of 2 mA cm^{-2}; (c) the areal specific capacitance *versus* different current densities (1–20 mA cm^{-2}); (d) Nyquist plots (the inset shows a magnified view of the high-frequency region).

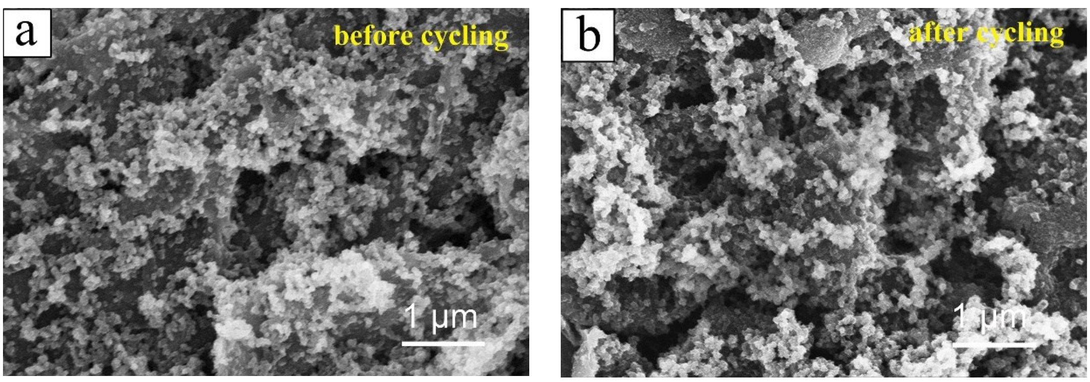

Fig. S16. The SEM images of the Lig/PANI/FGH/FCC electrode (a) before and (b) after 5000 charge/discharge cycles.

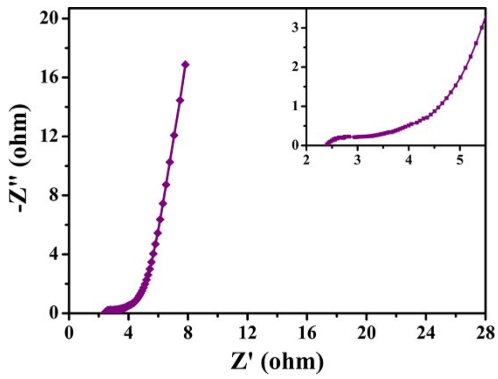

Fig. S17. Nyquist plots (the inset shows a magnified view of the high-frequency region) of Lig/PANI/FGH/FCC-based supercapacitor with PVA-H_2SO_4 as electrolyte.

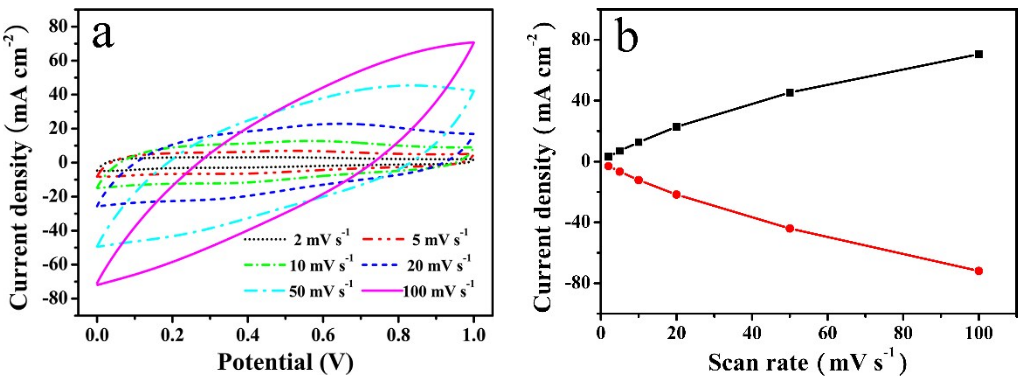

Fig. S18. (a) CV curves at different scan rates (2~100 mV s^{-1}), and (b) the relationship between the maximum current density and scan rate from CV curves for Lig/PANI/FGH/FCC-based supercapacitor with PVA-H_2SO_4 as electrolyte.

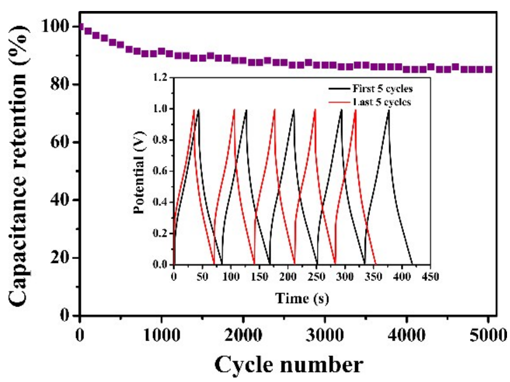

Fig. S19. Cycling stability of Lig/PANI/FGH/FCC-based all-solid-state supercapacitor at a current density of 20 mA cm^{-2}. The inset shows the GCD curves of first 5 cycles and last 5 cycles.

Table S1. The data of specific surface area and pore distribution for Lig/PANI/FGH and Lig/PANI.

Samples	BET surface area (m^2 g^{-1})			Total pore Volume (cc g^{-1})	Average pore size (nm)
	Total	S_{micro}	S_{meso}		
Lig/PANI/FGH	69.26	0	69.26	0.440	25.38
Lig/PANI	62.42	0	62.42	0.422	27.07

Table S2. The relative content (at.%) of N 1s species for FCC and FGH/FCC.

Samples	Pyridinic-N	amine moieties	Pyrrolic-N	Quaternary-N
Binding energy (eV)	398.8	399.5	400.2	401.1
FCC	21.8	26.8	41.8	9.6
FGH/FCC	26.5	24.0	27.1	22.4

Table S3. The relative content (at.%) of N 1s species for Lig/PANI/FGH/FCC.

Sample	=N-	-NH-	$-N^{+}-$
Binding energy (eV)	399	399.8	400.8
Lig/PANI/FGH/FCC	12.5	39.1	48.4

Table S4. Comparison of the areal capacitance of various electrodes in two-electrode system or corresponding conventional supercapacitors in aqueous electrolyte.

No.	Various electrodes	Areal capacitance (mF cm^{-2})	Energy density (μWh cm^{-2})	Power density (μW cm^{-2})	Reference
1	Lig/PANI/FGH/FCC	1223 (SSC) at 2 mA cm^{-2}	169.9	1000	This work
2	FGH/FCC	816 (SSC) at 1 mA cm^{-2}	113.3	500	This work
3	PANI/carbon cloth	787.4 at 2 mA cm^{-2}			[1]

4	Carbon textile/VC /VxOy	514 (SSC) at 2 mV s^{-1}			[2]
5	CNT-carbonized Cotton	1286 (SSC) at 1 mA cm^{-2}	124	2108	[3]
6	NC LDH NSs@Ag @CC	1133.3 at 1 mA cm^{-2}	78.8,40	785,12100	[4]
7	ACFC/MnO_2/CNT	2542 (SSC) at 2 mV s^{-1}	56.9	16287	[5]
8	PANI/CNT/air laid papers	1506 at 10 mA cm^{-2}	29.4	391	[6]
9	N-C/MnO_2 composites	183 at 0.5 mA cm^{-2}			[7]
10	PANi/CNT/PPWF	230 at 5 mA cm^{-2}			[8]
11	Photo Cotton fabric/CNT/MnO_2	480 (SSC) at 0.2 mA cm^{-2}			[9]
12	Graphene fiber fabrics	530 (1 mA cm^{-2})	47.1	400	[10]
13	Graphene–cellulose paper	81 at 1 mV s^{-1}	6	20	[11]
14	3D graphene network /MnO_2	1420 at 2 mV s^{-1}			[12]
15	Mn_3O_4/rGO nanohybrid paper	546.05 (ASC) at 1 mV s^{-1}			[13]
16	Co_3O_4 nanowire @MnO_2 on steel stainless substrate	710 at 4 mA cm^{-2}			[14]
17	EACC	756 at 6 mA cm^{-2}			[15]
18	CNF/CCS/PANI	1838.5 at 1 mA cm^{-2}			[16]
19	CNC-MWCNT-PPy	560 at 2 mA cm^{-2}			[17]
20	GN/AC/PPy	906 at 0.5 mA cm^{-2}			[18]
21	RGO/MnO_2 paper	897 at 50 mA g^{-1}	35.1	37.5	[19]
22	GO/PPy composite	377.6 at 0.2 mA cm^{-2}	13.2	4000	[20]
23	Graphene films	71 at 1 mA cm^{-2}	9.8	490	[21]
24	Graphene/carbon microspheres	160 (SSC) at 0.24 mA cm^{-2}	27	120	[22]
25	DN-PGH/$PANI_{PA}$	1744(SSC) at 0.5 mA cm^{-2}	155	200	[23]

ASC = Asymmetric Supercapacitors; SSC = Symmetric Supercapacitors. Nos. 3~7 are Carbon

Textile electrodes. Nos. 8~13 are other paper or fabric electrodes. Nos. 14~25 are other freestanding electrodes test in aqueous electrolyte.

Table S5. The electrical conductivity of different samples

Samples	Electrical conductivity ($S\ cm^{-1}$)
OCC	3.125
FGH/FCC	5.787
Lig/PANI/FGH/FCC	0.521
Lig/PANI/rOCC	0.160
Lig/PANI/rGO/rOCC	0.216

Table S6. Areal capacitance of various flexible electrodes/supercapacitors in the gel electrolyte.

No.	Various electrodes or devices	Areal capacitance ($mF\ cm^{-2}$)	Energy density ($\mu Wh\ cm^{-2}$)	Power density ($\mu W\ cm^{-2}$)	Reference
1	Lig/PANI/FGH/FCC	1156 (SSC) at 2 $mA\ cm^{-2}$	160.6	1000	This work
2	PANI-PVA hydrogel	420 (SSC) at 0.25 $mA\ cm^{-2}$			[24]
3	Polyaniline-PVA hydrogel	306 (SSC) at 0.25 $mA\ cm^{-2}$			[25]
4	PANI hydrogel	522 at 1 $mA\ cm^{-2}$	185		[26]
5	CC@RGO/PPy	985 (SSC) at 2 $mA\ cm^{-2}$	87.6	800	[27]
6	rGO@PANI carbon fabric electrode	790 at 1 $mA\ cm^{-2}$	28.21	120	[28]
7	fCC-PANI array-rGO	197 (SSC) at 0.1 $mA\ cm^{-2}$			[29]
8	PANI−Toray paper	1300 (SSC) at 10A g^{-1}			[30]
9	PANI/carbonized Modal textile	246.3 (SSC) at 10 $mV\ s^{-1}$			[31]
10	CF cloth / MnO_2 /	1050 (ASC) at 2 $mA\ cm^{-2}$			[32]

	polypyrrole	620 at 10 mA cm^{-2}			
11	Knitted CF cloth/ activated carbon particles	510 at 10 mV s^{-1}			33
12	T-Fe_2O_3/PPy NAs on carbon cloth	382.4 at 0.5 mA cm^{-2}			34
13	Dacron cloth supported $Cu(OH)_2$	195.8 (SSC) at 1 mA cm^{-2}	36	600	35
14	Polypyrrole/graphene/ $SnCl_2$ modified polyester textile	474 (SSC) at 1 mA cm^{-2}	65.8	500	36
15	Polyaniline/rGO/ polyester textile	781 (SSC) at 0.5 mA cm^{-2}	54	807	37
16	C-Web@Ni-Cotton fabric electrode	275.8(SSC) at 1 mA cm^{-2}			38
17	Polypyrrole coated air-laid paper	702 (SSC) at 1 mA cm^{-2}	62.4	420	39
18	Air-laid paper/CNT /MnO_2	123 at 1 mA cm^{-2}	4.2	200	40
19	Paper/graphite/PANI	356 at 0.5 mA cm^{-2}			41
20	Paper/PPy	420 (SSC) at 1 mA cm^{-2}			42
21	Graphene/polyaniline woven fabric	23(SSC) at 2 mA cm^{-2}	1.5	330	43
22	Metal−organic framework/conductive polymer hybrid fabric	206 (SSC) at 5 mV s^{-1}	12.8	2102	44
23	Ni foam/$NiCo_2O_4$ nanowire arrays	161 (SSC) at 1 mA cm^{-2}			45
24	PANI-PVH	718 (SSC) at 0.5 mA cm^{-2}			46
25	PANI-PCH film	488 (SSC) at 0.2 mA cm^{-2}	42	160	47

ASC = Asymmetric Supercapacitors; SSC = Symmetric Supercapacitors. Nos. 2~4 are PANI hydrogel electrodes which deposited on carbon cloth, Nos. 5~11 are carbon textile composites flexible electrodes, Nos. 12~23 are other paper or textile electrodes and other 3D porous electrodes with a large thickness. Nos. 24 and 25 are all-in-one supercapacitors.

References:

1 T. Liu, L. Finn, M. Yu, H. Wang, T. Zhai, X. Lu, Y. Tong, Y. Li, *Nano Lett.*, 2014, **14**, 2522-2527.

2 D. V. Lam, H. C. Shim, J. H. Kim, H. J. Lee, S. M. Lee, *Small*, 2017, **13**, 1702702.

3 M. Rana, S. Asim, B. Hao, S. Yang, P. C. Ma, *Adv. Sustainable Syst.*, 2017, **1**, 1700022.

4 S. C. Sekhar, G. Nagaraju, J. S. Yu, *Nano Energy*, 2017, **36**, 58-67.

5 L. Dong, C. Xu, Y. Li, C. Wu, B. Jiang, Q. Yang, E. Zhou, F. Kang, Q. H. Yang, *Adv. Mater.*, 2016, **28**, 1675-1681.

6 L. Dong, G. Liang, C. Xu, D. Ren, J. Wang, Z. Z. Pan, B. Li, F. Kang, Q. H. Yang, *J. Mater. Chem. A*, 2017, **5**, 19934-19942.

7 W. Fu, E. Zhao, X. Ren, A. Magasinski, G. Yushin, *Adv. Energy Mater.*, 2018, **8**, 1703454.

8 F. C. R. Ramirez, P. Ramakrishnan, Z. P. Flores-Payag, S. Shanmugam, C. A. Binag, *Synth. Met.*, 2017, **230**, 65-72.

9 L. Hu, M. Pasta, F. L. Mantia, L. Cui, S. Jeong, H. D. Deshazer, J. W. Choi, S. M. Han, Y. Cui, *Nano Lett.*, 2010, **10**, 708-714.

10 Z. Li, T. Huang, W. Gao, Z. Xu, D. Chang, C. Zhang, C. Gao, *ACS Nano*, 2017, **11**, 11056-11065.

11 Z. Weng, Y. Su, D. W. Wang, F. Li, J. Du, H. M. Cheng, *Adv. Energy Mater.*, 2011, **1**, 917-922.

12 Y. He, W. Chen, X. Li, Z. Zhang, J. Fu, C. Zhao, E. Xie, *Acs Nano*, 2013, **7**, 174.

13 Y. Hu, C. Guan, G. Feng, Q. Ke, X. Huang, J. Wang, *Adv. Funct. Mater.*, 2015, **25**, 7291-7299.

14 J. Liu, J. Jiang, C. Cheng, H. Li, J. Zhang, H. Gong, H. J. Fan, *Adv. Mater.*, 2011,

23, 2076-2081.

15 W. Wang, W. Liu, Y. Zeng, Y. Han, M. Yu, X. Lu, Y. Tong, *Adv. Mater.*, 2015, **27**, 3572-3578.

16 Q. Liu, S. Jing, S. Wang, H. Zhuo, L. Zhong, X. Peng, R. Sun, *J. Mater. Chem. A*, 2016, **4**, 13352-13362.

17 K. Shi, X. Yang, E. D. Cranston, I. Zhitomirsky, *Adv. Funct. Mater.*, 2016, **26**, 6437-6445.

18 L. Xu, M. Jia, Y. Li, S. Zhang, X. Jin, *RSC Adv.*, 2017, **7**, 31342-31351.

19 A. Sumboja, C. Y. Foo, X. Wang, P. S. Lee, *Adv. Mater.*, 2013, **25**, 2809-2815.

20 J. Cao, Y. Wang, J. Chen, X. Li, F. C. Walsh, J.-H. Ouyang, D. Jia, Y. Zhou, *J. Mater. Chem. A*, 2015, **3**, 14445-14457.

21 Z. Xiong, C. Liao, W. Han, X. Wang, *Adv. Mater.*, 2015, **27**, 4469-4475.

22 G. A. Ferrero, M. Sevilla, A. B. Fuertes, *Sustainable Energy & Fuels*, 2017, **1**, 127-137.

23 Y. Zou, R. Liu, W. Zhong, W. Yang, *J. Mater. Chem. A*, 2018, **6**, 8568-8578.

24 W. Li, H. Lu, N. Zhang, M. Ma, *ACS Appl. Mater. Interfaces*, 2017, **9**, 20142-20149.

25 W. Li, F. Gao, X. Wang, N. Zhang, M. Ma, *Angew. Chem. Int. Ed.*, 2016, **55**, 9196.

26 H. Heydari, M. B. Gholivand, *New J. Chem.*, 2017, **41**, 237-244.

27 Z. Chen, W. Liao, X. Ni, *Chem. Eng. J.*, 2017, **327**, 1198-1207.

28 Y. Lin, H. Zhang, W. Deng, D. Zhang, N. Li, Q. Wu, C. He, *J. Power Sources*, 2018, **384**, 278-286.

29 P. Du, Y. Dong, H. Kang, X. Yang, Q. Wang, J. Niu, S. Wang, P. Liu, *ACS Sustainable Chem. Eng.*, 2018, **6**, 14723-14733.

30 R. Soni, V. Kashyap, D. Nagaraju, S. Kurungot, *ACS Appl. Mater. Interfaces*, 2017, **10**, 676-686.

31 C. Wang, M. Zhang, K. Xia, X. Gong, H. Wang, Z. Yin, B. Guan, Y. Zhang, *ACS Appl. Mater. Interfaces*, 2017, **9**, 13331-13338.

32 J. Tao, N. Liu, L. Li, J. Su, Y. Gao, *Nanoscale*, 2014, **6**, 2922-2928.

33 K. Jost, D. Stenger, C. R. Perez, J. K. McDonough, K. Lian, Y. Gogotsi, G. Dion, *Energy Environ. Sci.*, 2013, **6**, 2698-2705.

34 L. Wang, H. Yang, X. Liu, R. Zeng, M. Li, Y. Huang, X. Hu, *Angew. Chem. Int. Ed.*, 2017, **56**, 1104-1110.

35 S. Lei, Y. Liu, L. Fei, R. Song, W. Lu, L. Shu, C. L. Mak, Y. Wang, H. Huang, *J. Mater. Chem. A*, 2016, **4**, 14781-14788.

36 X. Li, R. Liu, C. Xu, Y. Bai, X. Zhou, Y. Wang, G. Yuan, *Adv. Funct. Mater.*, 2018, **28**, 1800064.

37 H. Sun, S. Xie, Y. Li, Y. Jiang, X. Sun, B. Wang, H. Peng, *Adv. Mater.*, 2016, **28**, 8431-8438.

38 Q. Huang, L. Liu, D. Wang, J. Liu, Z. Huang, Z. Zheng, *J. Mater. Chem. A*, 2016, **4**, 6802-6808.

39 Y. Chen, K. Cai, C. Liu, H. Song, X. Yang, *Adv. Energy Mater.*, 2017, **7**, 1701247.

40 L. Dong, C. Xu, Y. Li, Z. Pan, G. Liang, E. Zhou, F. Kang, Q. H. Yang, *Adv. Mater.*, 2016, **28**, 9313-9319.

41 B. Yao, L. Yuan, X. Xiao, J. Zhang, Y. Qi, J. Zhou, J. Zhou, B. Hu, W. Chen, *Nano Energy*, 2013, **2**, 1071-1078.

42 L. Yuan, B. Yao, B. Hu, K. Huo, W. Chen, J. Zhou, *Energy Environ. Sci.*, 2013, **6**, 470-476.

43 X. Zang, X. Li, M. Zhu, X. Li, Z. Zhen, Y. He, K. Wang, J. Wei, F. Kang, H. Zhu, *Nanoscale*, 2015, **7**, 7318-7322.

44 K. Qi, R. Hou, S. Zaman, Y. Qiu, B. Y. Xia, H. Duan, *ACS Appl. Mater. Interfaces*,

2018, **10**, 18021-18028.

45 Q. Wang, X. Wang, B. Liu, G. Yu, X. Hou, D. Chen, G. Shen, *J. Mater. Chem. A*, 2013, **1**, 2468-2473.

46 F. Liu, J. Wang, Q. Pan, *J. Mater. Chem. A*, 2018, **6**, 2500-2506.

47 K. Wang, X. Zhang, C. Li, X. Sun, Q. Meng, Y. Ma, Z. Wei, *Adv. Mater.*, 2015, **27**, 7451-7457.